Macroscopic Modeling for Urban Low-Altitude Airspace Using Projected-Speed: Theory and Estimation

Ran Chen[1], Can Chen[1], and Nikolas Geroliminis*[1]

[1]Urban Transport Systems Laboratory (LUTS), EPFL, Lausanne, Switzerland

Short summary

The growth of Low-Altitude Air Transport (LAAT) systems calls for effective macroscopic modeling and control tools to manage dense drone traffic. Although the Macroscopic Fundamental Diagram (MFD) provides a useful framework for large-scale ground traffic analysis, its conventional formulations do not directly account for the three-dimensional interactions and path deviations that characterize drone operations. To address this issue, we introduce the concept of projected speed, which maps drone motion onto the shortest origin–destination path while preserving time-invariant trip lengths. Under this setting, we establish, with suitable assumptions, the theoretical validity of both accumulation-based and trip-based models for LAAT systems. In particular, we show that the accumulation-based model is exact at steady state, and that its mismatch under congestion is mainly caused by its inability to correctly capture transient dynamics rather than by trip-length heterogeneity itself. We then evaluate these models through extensive numerical experiments in a decentralized conflict-avoidance environment. The results verify that the proposed macroscopic models formulated in the projected space can be successfully applied to LAAT traffic and reproduce behaviors similar to those observed in ground transportation under a range of operating conditions, including hysteresis. These findings clarify the theoretical basis of macroscopic LAAT models and support their use for real-time estimation and airspace operations.
Keywords: Urban Air Mobility; Low-Altitude Air Transport; Macroscopic Fundamental Diagram

1 Introduction

Urban Air Mobility (UAM) has emerged as a promising approach to contemporary urban transportation challenges. In particular, the rapid development of unmanned aerial vehicles (UAVs) and Low-Altitude Air Transport (LAAT) systems has stimulated growing interest in monitoring, passenger transport, and cargo applications (Straubinger et al., 2020). In this new era, UAVs equipped with high-resolution cameras act as high-quality monitoring sensors, providing unique datasets for traffic models (Kim et al., 2024; Tak et al., 2025; Xiong et al., 2025). Large-scale field experiments have demonstrated the potential of massive drone data in capturing urban traffic dynamics (Barmpounakis & Geroliminis, 2020; Paipuri et al., 2021; Fonod et al., 2025). Beyond monitoring, UAM for modern on-demand services and logistics is emerging as a vital application, particularly for time-sensitive goods such as medical supplies and e-commerce packages (Li et al., 2020; Archetti et al., 2022).

Unlike ground traffic, LAAT dynamics involve multi-agent interactions in a three-dimensional space without the structural constraints of lanes or signals. As traffic density increases, microscopic conflict management becomes computationally demanding, making macroscopic modeling essential for scalable operations. In this context, the Macroscopic Fundamental Diagram (MFD), which relates total agent accumulation to aggregate outflow, provides a natural foundation (Daganzo, 2007; Geroliminis & Daganzo, 2008). In a single-reservoir setting, the dynamics are described by a conservation equation in which the outflow is determined by the MFD function; this is referred to as the *accumulation-based* (AB) model. However, the AB model, while suitable under slowly varying conditions, becomes overly restrictive when demand evolves rapidly, as demonstrated in Mariotte et al. (2017). This limitation arises because the model relies exclusively on instantaneous accumulation and speed, failing to capture historical information or transient trip dynamics. To address this limitation, Arnott (2013) introduced the bathtub model, and later Daganzo & Lehe (2015); Lamotte & Geroliminis (2018) proposed a reformulation of single-reservoir dynamics that explicitly accounts for variable trip lengths. This formulation, referred to as the *trip-based* (TB)

model, has been shown to provide more accurate predictions during transient phases and greater flexibility in handling heterogeneous trips within the same reservoir.
Despite established MFD-like behavior for LAAT systems analogous to ground traffic (Haddad et al., 2021; Safadi et al., 2023), conventional macroscopic formulations still struggle to capture the distinctive inefficiencies of three-dimensional flight, including high-dimensional conflicts, path elongation, and strong speed heterogeneity. More broadly, both the theory and application of such macroscopic models in LAAT systems remain relatively underexplored. Motivated by these observations, this paper revisits macroscopic outflow modeling for LAAT systems from both accumulation-based and trip-based perspectives. First, we introduce projected speed, defined as the true speed projected onto the shortest origin-destination (OD) path. This allows the trip length in the macroscopic model to be identified with the time-invariant shortest path, thereby removing the effect of time evolution from the trip-length term. Second, we provide a statistical derivation of the AB model and prove its exactness, under this setting, at the steady state. We further demonstrate that the model's accuracy degrades when the airspace is non-stationary, a limitation stemming directly from its failure to capture transient dynamics. Third, we revisit the TB model as a benchmark and propose real-time outflow estimators, which are then verified and evaluated numerically in a microscopic LAAT simulation environment.
The remainder of the paper is organized as follows. Section 2 introduces the macroscopic modeling framework, derives the accumulation-based formulation, and presents the implementation of the trip-based model for LAAT systems. Section 3 discusses the numerical experiments and compares the proposed estimators under different traffic conditions. Finally, Section 4 concludes the paper and discusses future research directions.

2 Methodology

This section develops the macroscopic modeling framework for LAAT systems. We first introduce the concept of *projected speed*, which maps three-dimensional flight dynamics onto a time-invariant one-dimensional distance representation, and then analyze the AB and TB models.

Introducing the Projected Speed

Macroscopic models are typically formulated using speed and trip length. Suppose drone i travels for τ_i, exits the airspace at time t_i, and has instantaneous true speed $\nu_i(t)$ at time t. Its actual trip length a_i and trip-average true speed μ_i satisfy

$$a_i = \int_{t_i-\tau_i}^{t_i} \nu_i(s)\, ds, \qquad \mu_i = \frac{1}{\tau_i} \int_{t_i-\tau_i}^{t_i} \nu_i(s)\, ds. \tag{1}$$

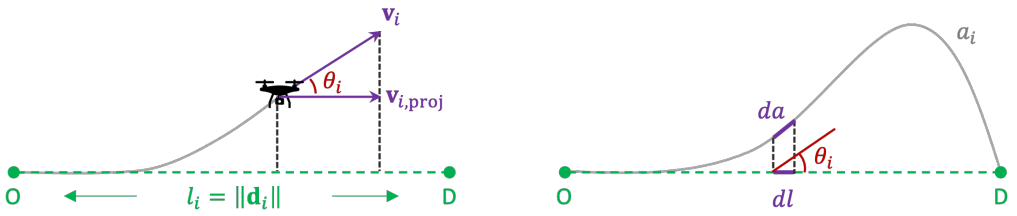


Figure 1: Kinematic illustration of projected speed relative to the true velocity and the OD path. Bold symbols ($\mathbf{v}_i$, etc.) denote vectors, whereas non-bold symbols (l_i, etc.) denote scalars.

In LAAT systems, however, the actual trip length a_i depends on local collision-avoidance maneuvers, and is therefore difficult to determine in real time, making the pair (a_i, μ_i) impractical for macroscopic estimation. To overcome this issue, we introduce the **projected speed**, defined as the component of velocity along the OD direction. As illustrated in Fig. 1, let $\theta_i(t)$ denote the angle between the true velocity $\mathbf{v}_i(t)$ and the OD vector $\mathbf{d}_i$, and let $v_i(t)$ denote the instantaneous projected speed, which can then be computed as

$$v_i(t) = \nu_i(t)\cos(\theta_i(t)) = \frac{\mathbf{v}_i(t)^\top \mathbf{d}_i}{\|\mathbf{d}_i\|}. \tag{2}$$

Using projected speed, the shortest OD length $l_i = \|\mathbf{d}_i\|$ and the trip-average projected speed u_i satisfy

$$l_i = \int_{t_i-\tau_i}^{t_i} v_i(s)\, ds, \qquad u_i = \frac{1}{\tau_i}\int_{t_i-\tau_i}^{t_i} v_i(s)\, ds. \tag{3}$$

Thus, path deviations are absorbed into a reduction in the projected speed, while the trip length is identified with the time-invariant OD distance. Importantly, this transformation preserves the travel time, since by construction

$$\tau_i = \frac{a_i}{\mu_i} = \frac{l_i}{u_i}. \tag{4}$$

Therefore, the projected representation is equivalent to the true-motion representation for the accumulation-based and trip-based models considered in this paper, both of which are formulated through the travel time τ. The advantage is that the projected formulation replaces the practically intractable actual path length a_i with the fixed and observable OD distance l_i. For convenience, the notation is summarized in Table 1.

Table 1: Notation for true-motion and projected quantities.

True-motion quantity†	Projected quantity‡
a_i: actual traveled path length	l_i: shortest OD length
ν_i: instantaneous true speed	v_i: instantaneous projected speed
μ_i: trip-average true speed	u_i: trip-average projected speed

† *realized motion along trajectory*

‡ *effective progress along the OD direction*

Note projected speed may become negative when a drone moves temporarily away from its destination, for example during a detour or conflict-avoidance maneuver.

Statistical Derivation of the Accumulation-Based Model

This section derives the AB model and discusses its limitation under transient conditions. We adopt the following assumptions:

- **Drone characterization:** Each drone i is characterized by its nominal trip length l_i and trip-average projected speed u_i, viewed as realizations of a joint random variable (l, u).
- **Time-invariant trip lengths:** The generated trip length l follows a stationary distribution $f_L(l)$.
- **Steady-state speed distributions:** At steady state with constant accumulation n^*, the trip-average projected speed u follows a stationary distribution, denoted by $f_{U|n^*}(u)$.

For a trip type (l, u), the travel time is deterministic as $\tau = l/u$. Let $\tilde{f}_t(l, u)$ denote the generation joint PDF of trip length and trip-average projected speed at time t. For a time-varying inflow $Q(t)$, a trip of type (l, u) generated at time s remains active at time t if and only if $t - s < \tau(l, u)$. Therefore, the number of active trips of type (l, u) at time t is

$$dn_t(l, u) = \left(\int_{t-\tau(l,u)}^{t} \tilde{f}_s(l, u)\, Q(s)\, ds\right) dl du. \tag{5}$$

Define the type-wise inflow density as

$$q_t(l, u) := \tilde{f}_t(l, u)\, Q(t). \tag{6}$$

Then the total accumulation is

$$n(t) = \iint \left(\int_{t-\tau}^{t} q_s(l, u)\, ds\right) dl du. \tag{7}$$

Normalizing by $n(t)$ gives the snapshot joint PDF

$$\tilde{g}_t(l, u) = \frac{\int_{t-\tau}^{t} q_s(l, u)\, ds}{n(t)}. \tag{8}$$

At steady-state, where $Q(t) = Q^*$, $\dot{n}(t) = 0$, and $n(t) = n^*$, the independence assumption yields the separable generation PDF

$$\tilde{f}_t(l, u) = f_L(l)\, f_{U|n^*}(u), \tag{9}$$

and the expectation of $\tau = l/u$ becomes

$$\mathbb{E}_{f|n^*}[\tau] = \mathbb{E}_{f|n^*}[l/u] = \mathbb{E}_f[l]\ \mathbb{E}_{f|n^*}[1/u]. \tag{10}$$

Accordingly, Eqs. (6)–(8) reduce to

$$q_t(l, u) = Q^* f_L(l)\, f_{U|n^*}(u), \tag{11}$$

$$n^* = Q^* \iint \tau\, f_L(l)\, f_{U|n^*}(u)\, dl du = Q^* \mathbb{E}_{f|n^*}[\tau], \tag{12}$$

and

$$\tilde{g}_t(l, u) = g_L(l)\, g_{U|n^*}(u) = \frac{\tau Q^* f_L(l)\, f_{U|n^*}(u)}{n^*}. \tag{13}$$

Combining Eqs. (10), (12), and (13), the steady-state snapshot mean speed is

$$\begin{aligned} \mathbb{E}_{g|n^*}[u] &= \iint u \cdot \frac{\tau Q^* f_L(l) f_{U|n^*}(u)}{n^*}\, dl du \\ &= \frac{Q^* \iint u \cdot l/u \cdot f_L(l) f_{U|n^*}(u)\, dl du}{\mathbb{E}_{f|n^*}[\tau]} \\ &= \frac{\iint l \cdot f_L(l) f_{U|n^*}(u)\, dl du}{\mathbb{E}_f[l]\mathbb{E}_{f|n^*}[1/u]} \\ &= \frac{1}{\mathbb{E}_{f^*}[1/u]}. \end{aligned} \tag{14}$$

The steady-state accumulation-based outflow can therefore be written as

$$G^* = Q^* = \frac{n^*}{\mathbb{E}_{f^*}[\tau]} = \frac{n^*}{\mathbb{E}_f[l]\mathbb{E}_{f^*}[1/u]} = n^* \frac{\mathbb{E}_{g|n^*}[u]}{\mathbb{E}_f[l]}, \tag{15}$$

where n^* is the steady-state accumulation, $\mathbb{E}_f[l]$ is the generation mean trip length, and $\mathbb{E}_{g|n^*}[u]$ is the steady-state snapshot mean of the trip-average projected speed. Since $\mathbb{E}_{g|n^*}[u]$ is generally not directly measurable, we can approximate it by the mean instantaneous projected speed $\mathbb{E}_{g|n^*}[v]$, and then estimate the latter by the measured space-mean speed over a window ΔT. At the same time, $\mathbb{E}_f[l]$ is estimated by the average OD path length. Thus,

$$\mathbb{E}_{g|n(t)}[v] \approx \hat{V}(t, \Delta T) = \frac{\sum_{i \in \mathcal{A}(t,\Delta T)} d_i}{\sum_{i \in \mathcal{A}(t,\Delta T)} t_i}, \quad \mathbb{E}_f[l] \approx \hat{L} = \frac{1}{|\mathcal{D}|} \sum_{i \in \mathcal{D}} l_i, \tag{16}$$

where $\mathcal{A}(t, \Delta T)$ is the set of drones active during $(t - \Delta T, t)$, d_i is the projected traveled distance of drone i during that window, t_i is its active time in the same window, $\mathcal{D}$ is the set of all drones, and $|\mathcal{D}|$ is its cardinality. The approximation is justified if the measurement window ΔT is chosen properly, such that the time-averaged instantaneous speed of each drone

$$\bar{v}_i = \frac{1}{t_i} \int_{t-\Delta T}^{t} v_i(s)\, ds \tag{17}$$

becomes a reasonable approximation of its trip-average speed u_i whenever the window captures a sufficient portion of its trip, and in particular when ΔT is of the order of τ. In that case, the corresponding weighted average over all active drones satisfies

$$\hat{V}(t, \Delta T) = \frac{\sum_{i \in \mathcal{A}(t,\Delta T)} \bar{v}_i\, t_i}{\sum_{i \in \mathcal{A}(t,\Delta T)} t_i} \approx \frac{\sum_{i \in \mathcal{A}(t,\Delta T)} u_i\, t_i}{\sum_{i \in \mathcal{A}(t,\Delta T)} t_i} \approx \mathbb{E}_{g|n(t)}[u]. \tag{18}$$

Accordingly, the practical estimate of Eq. (15) is

$$\hat{G}_{\mathrm{AB}}(n(t)) = n(t) \frac{\hat{V}(t, \Delta T)}{\hat{L}}, \tag{19}$$

provided that the system is at or sufficiently close to steady-state. The above derivation provides a statistical foundation for the accumulation-based MFD and shows that trip-length heterogeneity affects the steady-state relation only through its expectation, consistent with Lamotte et al. (2018); Laval (2023).

The next step is to understand why this equivalence breaks down under non-stationary conditions. Since trips of type (l, u) generated at $t - \tau(l, u)$ complete at t, the true outflow is

$$G_0(t) = \iint Q(t-\tau)\tilde{f}_{t-\tau}(l,u)\,dl\,du = \iint q_{t-\tau}(l,u)\,dl\,du. \tag{20}$$

Equation (20) can be viewed as a distributed-delay trip-based model. Accordingly, the error of the practical AB estimate can be written as

$$\begin{aligned}
\Delta_{\mathrm{AB}}(t) &= \hat{G}_{\mathrm{AB}}(t) - G_0(t) \\
&= \frac{n(t)}{\mathbb{E}_f[l]}\mathbb{E}_{g|n(t)}[v] - \iint q_{t-\tau}(l,u)\,dl\,du \\
&= \frac{n(t)}{\mathbb{E}_f[l]}\left(\mathbb{E}_{g|n(t)}[v] - \mathbb{E}_{g|n(t)}[u]\right) + \frac{n(t)}{\mathbb{E}_f[l]}\mathbb{E}_{g|n(t)}[u] - \iint q_{t-\tau}(l,u)\,dl\,du \\
&= \underbrace{\frac{n(t)}{\mathbb{E}_f[l]}\left(\mathbb{E}_{g|n(t)}[v] - \mathbb{E}_{g|n(t)}[u]\right)}_{\text{instantaneous-speed substitution bias}} + \underbrace{\iint \left(\frac{l}{\mathbb{E}_f[l]}\cdot \bar{q}_t(l,u) - q_{t-\tau}(l,u)\right) dl\,du}_{\text{cohort-averaging bias}},
\end{aligned} \tag{21}$$

where

$$\bar{q}_t(l,u) := \frac{1}{\tau(l,u)}\int_{t-\tau(l,u)}^{t} q_s(l,u)\,ds. \tag{22}$$

Hence, the transient error of the AB model can be interpreted as the sum of two components. The first term appears because the estimator replaces the trip-average speed u by the instantaneous speed v. At steady-state, one may expect $v \approx u$, while during a charging phase the current speed of an active drone may exceed its trip-average speed, since the remaining part of the trip is experienced under higher accumulation. Although this need not hold for every drone, it is natural to expect on average that

$$\mathbb{E}_{g|n(t)}[v] \geq \mathbb{E}_{g|n(t)}[u] \quad \text{during fast charging } (\dot{n} \gg 0), \tag{23}$$

which introduces a positive bias. The second term, namely the cohort-averaging bias, is intrinsic to the AB formulation itself: the true outflow depends on the cohort intensity $q_{t-\tau}(l,u)$ at departure, whereas the AB model replaces it by the travel-time average $\bar{q}_t(l,u)$. Therefore, during fast charging, recently generated slower cohorts tend to be overweighted, leading to overestimation, and vice versa. Importantly, even in the special case where all drones have identical trip length, i.e. $l \equiv \bar{L}$, the AB error remains

$$\Delta_{\mathrm{AB}}^{\bar{L}}(t) = \frac{n(t)}{\bar{L}}\left(\mathbb{E}_{g|n(t)}[v] - \mathbb{E}_{g|n(t)}[u]\right) + \int \left(\bar{q}_t(u) - q_{t-\tau}(u)\right)\,du, \tag{24}$$

which is generally nonzero when the system is not at steady-state. This proves that the main limitation of the accumulation-based model lies in its inability to correctly capture transient dynamics, rather than in trip-length heterogeneity.

Trip-Based Model and Real-Time Estimation

As a comparison with the AB model, we implement a trip-based (TB) formulation that explicitly captures transient dynamics through the remaining-distance dynamics

$$r_i(t) = l_i - \int_{t_{0,i}}^{t} v_i(s)\,ds. \tag{25}$$

Trip i is completed when $r_i(t) = 0$. Eq. (25) gives the exact remaining-distance dynamics, but can be implemented only when both the trip length l_i and instantaneous projected speed $v_i(t)$ are available; it therefore mainly serves as a conceptual benchmark. In the present LAAT setting, each OD length l_i is known a priori, whereas only an aggregate projected speed estimate is assumed measurable in real time. We therefore adopt a heterogeneous-trip-length, representative-speed setting, where each drone i retains its own trip length l_i but shares the same representative projected

speed $\hat{V}(t)$. Hence, if drone i enters the airspace at time $t_{0,i}$, its estimated remaining distance at time t is

$$\hat{r}_i(t) = l_i - \int_{t_{0,i}}^{t} \hat{V}(s)\, ds. \tag{26}$$

Equivalently, the estimated travel time $\hat{\tau}_i$ satisfies

$$\int_{t_{0,i}}^{t_{0,i}+\hat{\tau}_i} \hat{V}(s)\, ds = l_i. \tag{27}$$

To enable real-time estimation, we discretize time with step T_s and define

$$t_k = kT_s, \qquad k \in \mathbb{N}. \tag{28}$$

At time t_k, the available speed history is

$$\hat{V}_{[0:t_k]} = [\hat{V}(0), \hat{V}(t_1), \ldots, \hat{V}(t_k)]^\top, \quad \hat{V}(\cdot) \text{ obtained by Eq. (16).} \tag{29}$$

The estimator is implemented recursively. At time t_k, the inputs are the representative projected speed $\hat{V}(t_{k-1})$, current active set $\mathcal{A}(t_{k-1})$, total completed set $\mathcal{C}(t_{k-1})$, and estimated remaining-distance vector $\hat{\mathbf{r}}(t_{k-1})$ at the last step t_{k-1}. Information of all individual trip lengths l_i and the entry times $t_{0,i}$ are assumed provided beforehand. The algorithm is given below.

Algorithm 1 Real-time trip-based outflow estimation under heterogeneous lengths

Input: $\hat{V}(t_{k-1})$, $\mathcal{A}(t_{k-1})$, $\mathcal{C}(t_{k-1})$, $\hat{\mathbf{r}}(t_{k-1})$

Output: $\hat{G}(t_k)$, $\mathcal{A}(t_k)$, $\mathcal{C}(t_k)$, $\hat{\mathbf{r}}(t_k)$

Initialize $N_{\text{exit}} \leftarrow 0$, $\mathcal{A}(t_k) \leftarrow \mathcal{A}(t_{k-1})$, $\mathcal{C}(t_k) \leftarrow \mathcal{C}(t_{k-1})$, $\hat{\mathbf{r}}(t_k) \leftarrow \hat{\mathbf{r}}(t_{k-1})$
for each drone $i = 1, \ldots, m$ **do**
    if $i \in \mathcal{A}(t_k)$ **then**
        $\hat{r}_i(t_k) \leftarrow \hat{r}_i(t_{k-1}) - \hat{V}(t_{k-1}) \cdot T_s$
        if $\hat{r}_i(t_k) \le 0$ **then**
            $N_{\text{exit}} \leftarrow N_{\text{exit}} + 1$
            $\mathcal{A}(t_k) \leftarrow \mathcal{A}(t_k) \setminus \{i\}$
            $\mathcal{C}(t_k) \leftarrow \mathcal{C}(t_k) \cup \{i\}$
        end if
    else if $t_k \ge t_{0,i}$ **and** $i \notin \mathcal{C}(t_k)$ **then**
        $\mathcal{A}(t_k) \leftarrow \mathcal{A}(t_k) \cup \{i\}$
        $\hat{r}_i(t_k) \leftarrow l_i$
    end if
end for
$\hat{G}(t_k) \leftarrow N_{\text{exit}}/T_s$

Note that the representative-speed closure should not be viewed as a methodological deficiency. Rather, it defines the practically relevant estimation problem under limited observability. The contribution here is to show that even under the more general aggregate-speed setting, the TB estimator remains highly accurate, as demonstrated in Section 3.

3 Numerical Results

This section evaluates the proposed outflow estimation framework through numerical experiments. We introduce the simulation setup before comparing the AB and TB estimates under monotone loading and loading-unloading conditions, with emphasis on congestion and hysteresis.

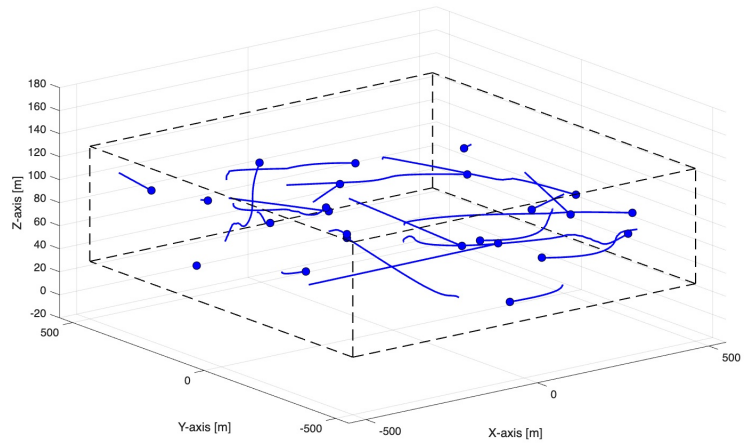


Figure 2: Three-dimensional snapshot of the simulation. The individual trajectories illustrate the maneuvers required to maintain safety region within the constrained airspace.

Simulation Configuration

The numerical experiments are conducted using the LAAT modeling framework developed in Safadi et al. (2023), which employs a force-field-based decentralized collision avoidance scheme Quan et al. (2021). The simulated airspace is a three-dimensional domain of size $1000 \times 1000 \times 100$ [m^3], and a representative trajectory snapshot is shown in Fig. 2. Each drone departs from a randomly generated origin and travels toward a randomly generated destination. The nominal route is the straight line connecting the two points, while the realized trajectory is continuously adjusted according to the dynamics

$$\dot{\mathbf{p}}_i(t) = \mathbf{v}_i(t), \tag{30}$$

$$\dot{\mathbf{v}}_i(t) = -\mathbf{K}\big(\mathbf{v}_i(t) - \mathbf{v}_{i,c}(t)\big), \tag{31}$$

where $\mathbf{p}_i(t)$ and $\mathbf{v}_i(t)$ denote the position and true velocity, respectively, and $\mathbf{K}$ is a given control gain matrix. The commanded velocity $\mathbf{v}_{i,c}(t)$ is computed as

$$\mathbf{v}_{i,c} = \mathrm{sat}\left(\mathrm{sat}\big(\phi_{i,\mathrm{att}}(\mathbf{p}_i, \mathbf{v}_i), V_{\max}\big) + \sum_{j \in \mathcal{N}_i} \phi_{i,\mathrm{rep}}(\mathbf{p}_i, \mathbf{p}_j), V_{\max}\right). \tag{32}$$

Here, $\phi_{i,\mathrm{att}}$ denotes the attractive component, which depends on the current state $(\mathbf{p}_i, \mathbf{v}_i)$ and always points toward the destination, while $\phi_{i,\mathrm{rep}}$ is the repulsive component generated by neighboring drones $j \in \mathcal{N}_i$. The saturation operator $\mathrm{sat}(\cdot, V_{\max})$ bounds the commanded speed by $V_{\max}$. The simulation time step is $T_s = 0.5$ [s], and outflow measurements or estimates are made every $T_m = 60$ [s]. The maximum speed is set to $V_{\max} = 20$ [m/s]. The mean OD length is $\bar{L} = 532$ [m], obtained by Monte-Carlo sampling of random origin-destination pairs with samples shorter than 90 [m] discarded.

Results and Discussion: Free-Flow and Congestion

In the first experiment, the demand is continuously increased. The experiment is repeated 20 times with independently generated OD pairs. Fig. 3a shows the time evolution of the inflow $Q(t)$, the true outflow $G_0(t)$, and the accumulation $n(t)$. From $t = 0$ to 35 [min], the system is stable and the outflow follows the inflow with a slight delay, while the accumulation increases steadily, resulting in a quasi-steady-state regime. At $t = 35$ [min], the accumulation reaches the critical threshold $n_c \approx 140$ [a.c], marking the onset of congestion. Beyond this point, the outflow departs from the inflow and eventually collapses toward zero, while the accumulation rises rapidly, indicating a

trend toward gridlock. Fig. 3b is shown alongside these results for later discussion of the estimation errors.

The evolution of the mean true speed and mean projected speed, defined in Eq. (2), is shown in Fig. 3c. In the low-accumulation regime, the projected speed is nearly identical to the true speed since collision-avoidance maneuvers are rare. After congestion starts ($t = 35$ [min], $n = 140$ [a.c]), collision-avoidance interactions become frequent and the projected speed deviates significantly from the true speed. As n continues to increase, the projected speed approaches zero, indicating a near-gridlock state in which trip completions almost cease[1]. By contrast, the true speed remains non-zero, suggesting that drones continue to seek spatial vacancies but make little effective progress toward their destinations, due to the sub-optimality of the force-field method and the absence of intelligent route guidance.

Fig. 3d compares the true outflow with the AB and representative-speed TB estimates over time and accumulation, respectively. As congestion intensifies, the AB model progressively overestimates the outflow, whereas the TB model tracks the true response more closely, even under strong speed heterogeneity. Recall Eq. (21), in this simulation setting, the instantaneous-speed substitution bias of the AB model appears to remain small when the measurement window is chosen appropriately; the observed error is therefore likely dominated by the cohort-averaging bias, especially during charging and unloading transients. Quantifying the relative contribution of these two biases is beyond the scope of this paper and is left for future work.

To quantify the estimation performance, the relative error $\bar{\epsilon}(t)$ of the estimate $\hat{G}(t)$ with respect to $G_0(t)$ is defined as

$$\bar{\epsilon}(t) = \left(\frac{\hat{G}(t) - G_0(t)}{G_0(t)} \right) \times 100\%. \tag{33}$$

The error distribution is shown in Fig. 3b. In the free-flow regime, both models exhibit comparable accuracy. After $t = 40$ [min], however, the error of the AB estimate increases sharply, while the TB estimate remains noticeably more accurate.

Results and Discussion: Hysteresis

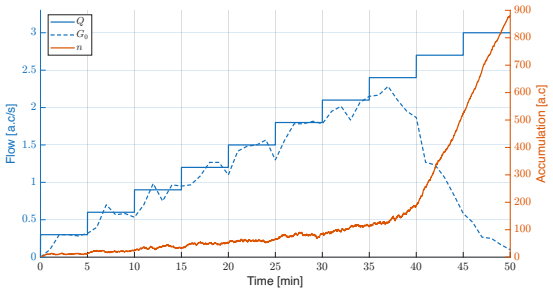
In the next experiment, we compare the AB and TB estimates under hysteresis. Only one realization is shown, since the system is chaotic and hysteresis may appear at different times even under the same demand profile. As shown in Fig.4a, the inflow first increases gradually and then decreases continuously to about 20% of the maximum inflow shortly after the airspace reaches critical accumulation. Fig.4c shows the corresponding speed dynamics. During loading, both the true and projected speeds decrease. Although unloading begins at $t = 25$ [min] with $n = 145$ [a.c], the speeds do not recover immediately but exhibit hysteresis due to spatial heterogeneity and local congestion. Once the accumulation drops to 55 [a.c] at $t = 32$ [min], the airspace is released and speeds recover toward free-flow values.

The hysteresis loops of the outflow are shown in Fig.4d. Although both models reproduce the loop qualitatively, the TB estimate follows the true response more closely, whereas the AB model underestimates the outflow during unloading, in agreement with the theoretical analysis. Finally, Fig.4b presents the time evolution of the relative errors for one experiment where the AB estimate shows larger fluctuations, indicating that the TB estimate is more robust.

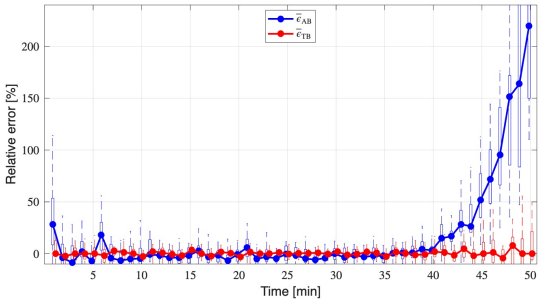
4 Conclusion

This paper revisits macroscopic outflow modeling for Low-Altitude Air Transport (LAAT) systems using both accumulation-based (AB) and trip-based (TB) methods. To account for the path-deviating nature of drone operations, we introduce the concept of projected speed, which allows three-dimensional flight dynamics to be mapped onto a time-invariant origin–destination distance. Under this setting, we derive the AB model from a statistical viewpoint and prove its exactness at steady state. The analysis further shows that the main limitation of the AB model is its inability to capture the exact transient dynamics. We then revisit the TB model and implement a real-time estimation algorithm. Numerical experiments in a microscopic LAAT simulation environment verify that both models formulated in the projected space perform well in free-flow conditions, whereas the TB model remains much more accurate and consistent under fast-changing dynamics.

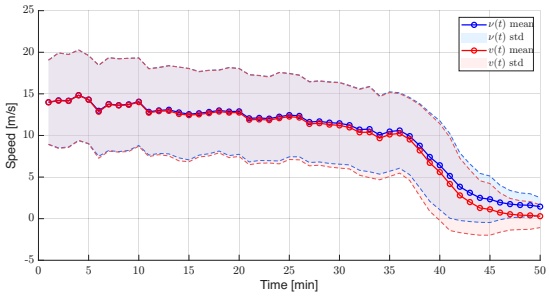
[1] A zero mean projected speed does not strictly imply zero completions. Some drones may reach their destinations while others move away due to collision avoidance, leading to a zero mean speed.

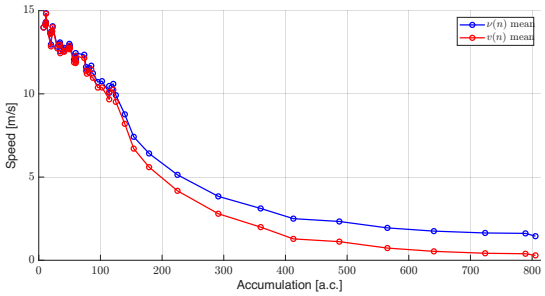


(a) Time evolution of inflow Q (blue solid), true outflow G_0 (blue dashed), and accumulation n (red solid).

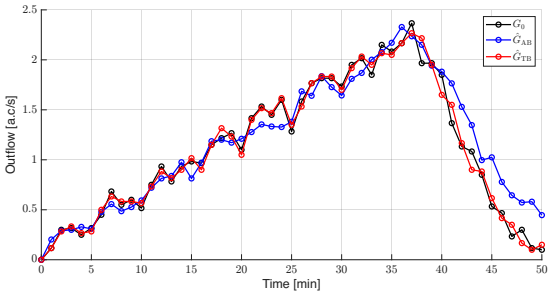


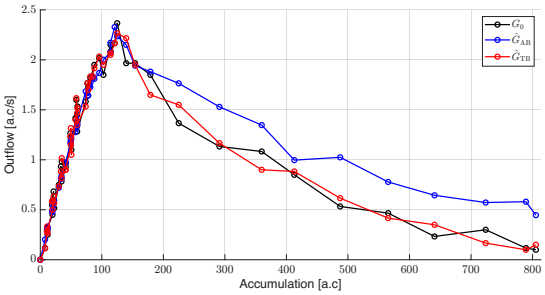
(b) Distribution of the relative estimation error $\bar{\epsilon}(t)$ over multiple experiments. Solid curves indicate the medians.





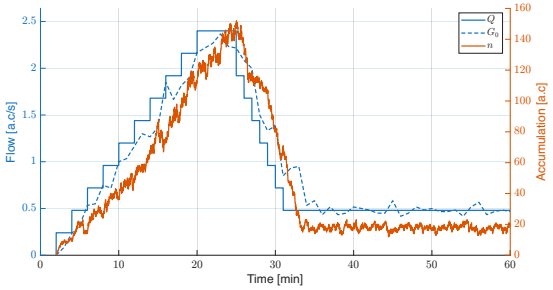
(c) Comparison of true speed ν (blue curves) and projected speed v (red curves): time evolution (left) and variation with accumulation (right). Solid curves denote the means, and the shaded regions show the standard-deviation bands in the time-domain plots only.



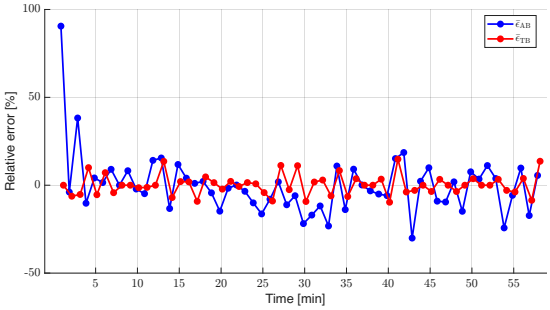


(d) Comparison of true and estimated outflows: time evolution (left) and variation with accumulation (right).

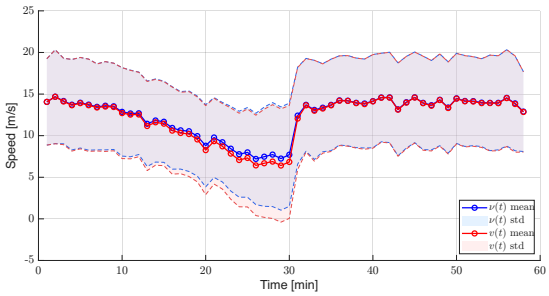
Figure 3: Comparison of trip-based and accumulation-based outflow estimation. Panels (a), (c), and (d) correspond to one representative experiment, while panel (b) summarizes the error distribution over all 20 experiments.

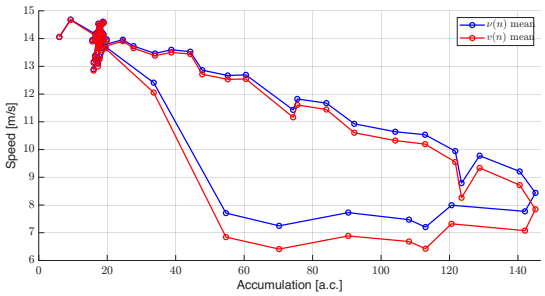


(a) Time evolution of Q, G_0, n during the loading–unloading process.

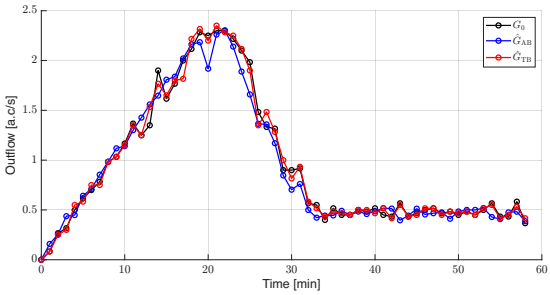


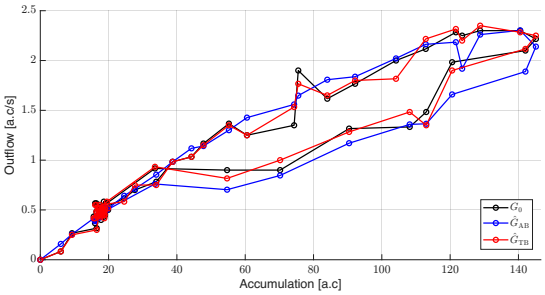
(b) Time evolution of the relative estimation error $\bar{\epsilon}(t)$ over one experiment.





(c) Hysteresis loops of the instantaneous true speed ν and instantaneous projected speed v: variation with time (left) and accumulation (right).





(d) Comparison of true and estimated outflows under hysteresis: variation with time (left) and accumulation (right).

Figure 4: Comparison of outflow estimation under hysteresis.

In particular, the simulations show that the AB model tends to overestimate the outflow during loading and underestimate it during unloading, in agreement with the theoretical predictions.
Future work will proceed in two directions. First, the numerical study will be strengthened through additional sensitivity analysis to further verify the robustness of the projected-space formulation, considering the variation of both operational parameters, such as speed limits and detection radii, and scenario settings, such as the measurement window and transient demand profiles. Second, the framework will be extended to a multi-class setting, where different types of drones are described by class-specific characteristics, and then integrated into real-time traffic management and control schemes, from dynamic departure management in a single region to model predictive perimeter control in a multi-regional setting.

Acknowledgements

This work was supported as a part of NCCR Automation, a National Centre of Competence in Research, funded by the Swiss National Science Foundation (grant number 51NF40_225155).

References

Archetti, C., Peirano, L., & Speranza, M. G. (2022). Optimization in multimodal freight transportation problems: A survey. *European Journal of Operational Research*, *299*(1), 1–20.

Arnott, R. (2013). A bathtub model of downtown traffic congestion. *Journal of Urban Economics*, *76*, 110–121.

Barmpounakis, E., & Geroliminis, N. (2020). On the new era of urban traffic monitoring with massive drone data: The pneuma large-scale field experiment. *Transportation research part C: emerging technologies*, *111*, 50–71.

Daganzo, C. F. (2007). Urban gridlock: Macroscopic modeling and mitigation approaches. *Transportation Research Part B: Methodological*, *41*(1), 49–62.

Daganzo, C. F., & Lehe, L. J. (2015). Distance-dependent congestion pricing for downtown zones. *Transportation Research Part B: Methodological*, *75*, 89–99.

Fonod, R., Cho, H., Yeo, H., & Geroliminis, N. (2025). Advanced computer vision for extracting georeferenced vehicle trajectories from drone imagery. *Transportation Research Part C: Emerging Technologies*, *178*, 105205.

Geroliminis, N., & Daganzo, C. F. (2008). Existence of urban-scale macroscopic fundamental diagrams: Some experimental findings. *Transportation Research Part B: Methodological*, *42*(9), 759–770.

Haddad, J., Mirkin, B., & Assor, K. (2021). Traffic flow modeling and feedback control for future low-altitude air city transport: An mfd-based approach. *Transportation Research Part C: Emerging Technologies*, *133*, 103380.

Kim, S., Tak, Y., Barmpounakis, E., & Geroliminis, N. (2024). Monitoring outdoor parking in urban areas with unmanned aerial vehicles. *IEEE Transactions on Intelligent Transportation Systems*, *25*(10), 13393–13406.

Lamotte, R., & Geroliminis, N. (2018). The morning commute in urban areas with heterogeneous trip lengths. *Transportation Research Part B: Methodological*, *117*, 794–810.

Lamotte, R., Murashkin, M., Kouvelas, A., & Geroliminis, N. (2018). Dynamic modeling of trip completion rate in urban areas with mfd representations. In *2018 trb annual meeting online* (pp. 18–06192).

Laval, J. A. (2023). Effect of the trip-length distribution on network-level traffic dynamics: Exact and statistical results. *Transportation Research Part C: Emerging Technologies*, *148*, 104036. Retrieved from `https://www.sciencedirect.com/science/article/pii/S0968090X23000256` doi: https://doi.org/10.1016/j.trc.2023.104036

Li, C.-l., Qu, W.-q., Li, Y.-d., Huang, L.-y., & Wei, P. (2020). Overview of traffic management of urban air mobility (uam) with evtol aircraft. *J. Traffic Transp. Eng*, *20*(4), 35–54.

Mariotte, G., Leclercq, L., & Laval, J. A. (2017). Macroscopic urban dynamics: Analytical and numerical comparisons of existing models. *Transportation Research Part B: Methodological*, *101*, 245–267.

Paipuri, M., Barmpounakis, E., Geroliminis, N., & Leclercq, L. (2021). Empirical observations of multi-modal network-level models: Insights from the pneuma experiment. *Transportation Research Part C: Emerging Technologies*, *131*, 103300.

Quan, Q., Fu, R., & Cai, K.-Y. (2021). Practical control for multicopters to avoid non-cooperative moving obstacles. *IEEE Transactions on Intelligent Transportation Systems*, *23*(8), 10839–10857.

Safadi, Y., Fu, R., Quan, Q., & Haddad, J. (2023). Macroscopic fundamental diagrams for low-altitude air city transport. *Transportation Research Part C: Emerging Technologies*, *152*, 104141.

Straubinger, A., Rothfeld, R., Shamiyeh, M., Büchter, K.-D., Kaiser, J., & Plötner, K. O. (2020). An overview of current research and developments in urban air mobility–setting the scene for uam introduction. *Journal of Air Transport Management*, *87*, 101852.

Tak, Y., Fonod, R., & Geroliminis, N. (2025). Deep learning for vehicle re-id in urban traffic monitoring with visual and temporal information. *Communications in Transportation Research*.

Xiong, W., Fonod, R., Alahi, A., & Geroliminis, N. (2025). Multi-source urban traffic flow forecasting with drone and loop detector data. *IEEE Transactions on Intelligent Transportation Systems*.